Molekul, Vol. 17. No. 2, July 2022: 200 – 211

MOLEKUL
eISSN: 2503-0310

Articles

https://doi.org/10.20884/1.jm.2022.17.2.5456

Gold (Au), Silver (Ag) and Bimetallic Au/Ag Core-Shell Nanoparticles: Synthesis and Applications in 4-Nitrophenol Reduction Reactions

Nurjannah[1], Bualkar Abdullah[1], Yuliati Herbani[2]*

[1]Department of Physics, Hasanuddin University, Makassar, 90245, Indonesia
[2]Research Center for Photonics, National Research and Innovation Agency (BRIN), Kawasan PUSPIPTEK, Tangerang Selatan, 15314, Indonesia

*Corresponding author email: yuliati.herbani@brin.go.id

Received February 05, 2022; **Accepted** May 23, 2022; **Available online** July 20, 2022

ABSTRACT. Au, Ag, and Au/Ag core-shell nanoparticles (NPs) were synthesized in aqueous solution by chemical reduction. UV-Vis absorption spectra confirmed a single surface plasmon resonance (SPR) peak for Au and Ag NPs, at 520 nm and 419 nm, respectively. Au/Ag core-shell NPs' UV-Vis spectra showed two distinct peaks at 385 and 480 nm, confirming a core-shell structure different from its alloy counterpart. Transmission electron microscopy (TEM) shows a relatively uniform spherical shape for both Au and core-shell Au/Ag NPs, while Ag NPs have a variety of forms such as a prism, rod, and spherical. The average size of the synthesized nanoparticles was quite similar, between 18 and 25 nm. The 4-nitrophenol reduction reaction model was used to study the catalytic ability of nanoparticles where Au/Ag core-shell NPs showed higher catalytic activity than the other monometallic NPs used in this study.

Keywords: Au-Ag/core-shell nanoparticles, catalytic activity, 4-nitrophenol.

INTRODUCTION

Gold (Au) and silver (Ag) plasmonic nanoparticles are nanomaterials with unique optical and electronic properties, which open up many opportunities in practical biomedical applications, such as therapeutic, diagnostic, and sensing applications (Feng et al., 2019; Das et al., 2011; Bijalwan et al., 2019). These nanoparticles have been studied very well and in detail, especially regarding the effect of size modification on plasmon absorption due to its catalytic activity (Link et al., 1999). Furthermore, metal nanoparticles can be deposited on various supports to establish a better overall efficiency of the catalytic process (Bijalwan et al., 2019) where the surface-to-volume ratio is high (Ahmad et al., 2019). In more detail, the application of gold nanoparticles (AuNP) is extended to various biomedical fields, such as biosensors, clinical chemistry, immunoassays, genomics, photo-thermolysis of cancer cells, detection and control of microorganisms, targeted drug delivery, optical imaging and monitoring of biological cells and tissues by utilizing resonance scattering or in vivo photoacoustic technique (Bijalwan et al., 2019; Jiang et al., 2020).

Nanoparticles derived from gold have medical and pharmaceutical applications (Shen et al., 2017). Because of their excellent ability to penetrate intercellular spaces, gold nanoparticles are used as carriers in cancer diagnosis (Bijalwan et al., 2019). They also have high stability and capacity, are protected from reduction, have controlled release of ions, have good tolerability (Shen et al., 2017), and are very compliant and safe in terms of safe dosage (Sardar et al., 2009). When stabilized or protected by shells, Nanoparticles show good stability in reducing aggregation processes and other decay modes. A protective layer on nano-sized particles is needed to increase the driving force in keeping the core particles from being finely scattered (Sardar et al., 2009; Umamaheswari et al., 2018).

The reduction of nitrophenol by borohydride in suitable catalysts has been widely applied (Saha et al., 2010; Sardar et al., 2009). The removal of 4-nitrophenol in the presence of catalytic Au and Ag monometallic nanoparticles has been one of the most extensively studied in this decade. However, the catalytic activity of the nanoparticle alloys showed a better reaction and stood out when compared to monometallic nanoparticles. The combination of properties displayed depends on the variety of constituents. Its catalytic activity can be attributed to the surface area and the presence of regions that have a higher electron density.

The emergency in global energy has necessitated the researchers on the advancement of contamination-free energy sources and practical solutions to the regular pollution of the environment (Azhar, 2019; Umamaheswari et al., 2018). 4-

nitrophenol (4-NP) is one of several toxic. Dangerous contaminants found in industrial and agricultural raw materials, which is a hazardous contributor to water pollutants because it is considered one of the most poisonous and refractory pollutants (Kuroda et al., 2009; Mahalakshmi et al., 2020; Nemanashi & Meijboom, 2013; Shen et al., 2017), has anthropogenic, toxic and inhibitory properties (Sarmah et al., 2015) that poses a severe threat to many ecosystems, water supplies and human health (Azhar, 2019). On the other hand, the reduced product, i.e., 4-aminophenol (4-AP), is less toxic and has an essential role as a photographic developer, corrosion inhibitor (inhibitor and lubricant), desiccant, and precursor for the manufacture of analgesic, antipyretic and industrial plastics (Sahu et al., 2020; Sarmah et al., 2015; Shen et al., 2017; H. Wang et al., 2005). However, the treatment of wastewater contaminated with 4-NP is not effective with ordinary conventional methods because of the high stability and solubility of 4-NP in water (Sarmah et al., 2015). Therefore, effective wastewater treatment is needed and does not require a long time in the reaction process. Compared to other metal catalysts, AuNP has attracted much attention due to its high catalytic activity in mild conditions, even at ambient or low temperatures (Saha et al., 2010). According to Haldar et al. 2014, the catalytic activity and efficiency of the Au-Ag/core-shell nanostructure in the reaction between 4-NP and NaBH4 in the formation of 4-AP rose as the Au-core size grew up to 96.5%. As a result, converting 4-NP to 4-AP serves a significant function in pollution reduction and resource regeneration. To date, considerable efforts have been made by applying metal nanoparticles to catalyze the reduction of 4-NP to 4-AP by $NaBH_4$, which is the most efficient way (Sahu et al., 2020; Shen et al., 2017; Wang et al., 2005). Many metal alloy nanoparticles have been reported to use as a catalyst in wastewater treatment. However, the application of noble metal particles (monometallic and bimetallic alloy particles) is still limited (Wang et al., 2019).

In this study, bimetallic Au-Ag/core-shell nanoparticles have been prepared using a chemical reduction method. By varying the volume of Au seed as a core and a constant volume of Ag ions, Ag ions could effectively grow up on the Au core to form the core-shell structure with the varying shell thickness. The excellent match of the lattice constant (the difference is 0.2%) of Ag and Au nanocrystal (Vinod & Gopchandran, 2014) also helps the deposition. This study will explore the optical absorption Au-Ag/core-shell nanoparticles as a function of Ag shell thickness. The catalytic properties of the monometallic (Au, AgNPs) and Au-Ag/core-shell NPs were then evaluated using a reduction reaction model of 4-NP with $NaBH_4$ as a reducing agent. Many researchers have used $NaBH_4$ as a reducing agent (Aditya et al., 2017; Wang et al., 2019; Neal et al., 2019), which very well managed to reduce 4-NP to 4-AP in a relatively fast time. As a result, it is believed that the findings of this research will highlight the critical function of bimetallic core-shell NPs in the catalytic reduction of 4-nitrophenol (4-NP) and their advantages over monometallic nanoparticles.

EXPERIMENTAL SECTION

Gold (III) chloride trihydrate ($HAuCl_4.3H_2O$, 99.9%, Sigma Aldrich), silver nitrate ($AgNO_3$, 98%, SmartLab), 4-nitrophenol (4-NP, 99.9 %, Merck), ascorbic acid ($C_6H_2O_6$, 99%, Merck), trisodium citrate ($Na_3C_6H_5O_7$, 99.9%, Merck), sodium borohydride ($NaBH_4$. 98%, Wako-Japan) were used in this work without further purification. All experiments used aqua bidest as a solvent. AuNPs were synthesized using a thermal method as follows. 1 mL gold (III) chloride trihydrate one wt.% aqueous solution and 2 mL trisodium citrate 38.8 mM aqueous solution was quickly added into aqua bidest 90 mL 90°C stir well. After the color changes to red-purple, the solution is immediately cooled in an ice bath. Ag NPs were also prepared by the same method. 0.018 g silver nitrate and 38.8 mM trisodium citrate 2 mL aqueous solution were added into aquabidest 100 mL 70°C. After the colour changes to bright yellow, the solution is cooled quickly into the ice bath. Au-Ag/core-shell were prepared using the following seed colloidal technique. In a typical experiment, some volumes of Au NPs (0.4, 1, 5, 10, 20, dan 40) mL were prepared as seed, and 1 mL trisodium citrate 38.8 mM solution were then added to 30 mL aqua bidest together with the seeds with continuous stirring. Then, 1.2 mL of 10 mM silver nitrate and 0.4 mL of 100 mM ascorbic acid aqueous solution were quickly added while stirring at 300 rpm for 10 minutes. UV-Vis spectroscopy (MayaPro 2000, Ocean Optics) and transmission electron microscopy (TEM, Tecnai G20 S-TWIN, Thermo Fisher Scientific) were used to confirm the formation and the microstructure of the resulting nanoparticles. Their particle size distributions were constructed utilizing free-software ImageJ, calculating for more than 300 particles.

The 4-NP catalytic reduction assay was prepared using a concentration of 0.015 M in 20μL volume. This assay was then added to 3 mL of aqua bidest. To start the reaction, 100μL of fresh sodium borohydride (0.01M stock solution) into the assay while constantly stirring at 200 rpm for some minutes. The resulting solution will immediately undergo a colour change from transparent to bright yellow. 100 μL of the synthesized nanoparticles (Au, Ag NPs, Au-Ag/core-shell) were then added separately into the reaction assay at room temperature as a catalyst. The catalytic reaction with these nanoparticles was monitored by measuring the UV-Vis absorbance spectrum of the reaction solution in the 200 to 600 nm wavelength range, with an increment acquisition time of 1 minute. The transformation of 4-NP to 4-aminophenol (4AP) is

an important organic component for synthesizing lubricants, drugs, and dyes (Mourya et al., 2018; Nemanashi & Meijboom, 2013).

The equation of time dependence of the absorbance of 4-nitrophenolate ions (Zhao et al., 2015):

$$In(A_t/A_0)(t) = In(A_t/A_0)(0) - k_r t \quad (3)$$

where the ratio (A_t/A_0) here is identical to the ratio of the concentration of 4-nitrophenolate at a time, t, to its concentration before the reaction starts, i.e. $A_t/A_0 = c/c_0$, and k_r is the reaction rate constant. From this plot we can also deduce the induction period, τ, upon which the absorbance is constant at a certain time after the reaction starts. Following Eq. (3), the induction period, τ, is defined as(Zhao et al., 2015):

$$\tau = In(A_t/A_0)(0)/k_r \quad (4)$$

RESULTS AND DISCUSSION

Au, Ag and Au/Ag Core-Shell Nanoparticles Synthesis

A complete equations to produce Au NPs is as follows (Anugrah Ilahi et al., 2021):

$$2HAuCl_4 + 4Na_2C_6H_5O_7 \rightarrow H_2 + 2Au^0 + 4CO_2 + 4Na_2C_6H_5O_5 + 8NaCl \quad (5)$$

The synthesized Au NPs showed a red-purple colour solution which proved that the expected nanoparticles had been generated (**Figure 1**). This fact can be confirmed by UV-Vis absorption measurement of the surface plasmon resonance (SPR) peak. The SPR band was observed due to the combined oscillation of the electron conduction band on the surface of the metal nanoparticles in resonance with light waves. The resulting SPR band at a wavelength of 520 nm showed that the expected gold nanoparticles had been successfully synthesized (**Figure 2**). Many studies have reported that the SPR absorption band of metal nanoparticles is related to the size, shape, and aggregation conditions (Umamaheswari et al., 2018). From **Figure 2**, it is expected that the shape of Au NPs was spherical because it has a single peak without dispersion at a longer wavelength. The TEM image confirmed this structure in **Figure 3** that most particles were spherical with particle size around 20 nm. The analysis of the particle size distribution of Au NPs using ImageJ resulted in an average diameter of (18.7 ± 8.8) nm.

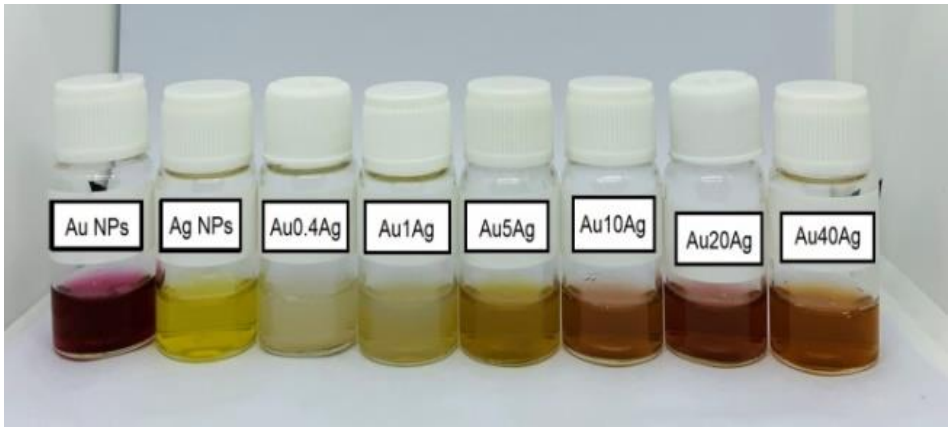

Figure 1. The photograph of the synthesized Au, Ag, and Au-Ag/core-shell NPs

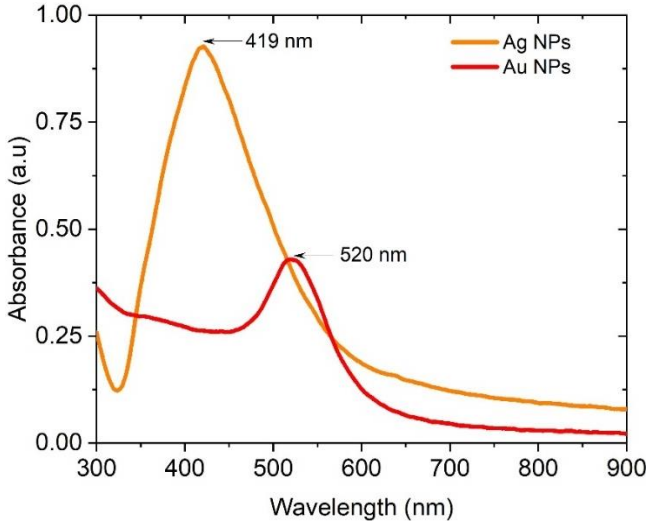

Figure 2. UV-Vis absorption spectra of Au (red) and Ag NPs (orange).

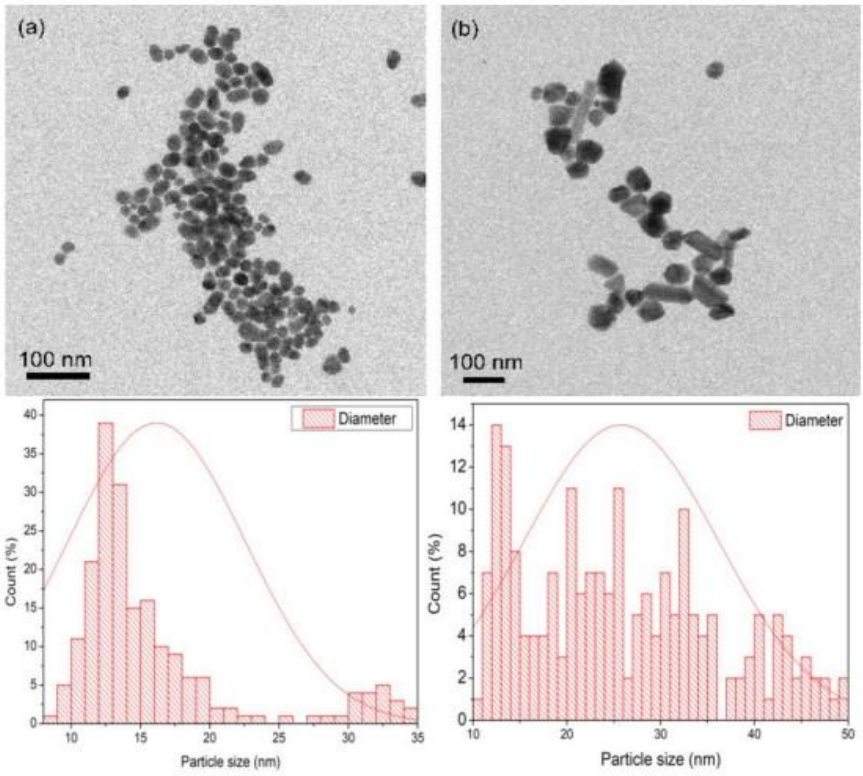

Figure 3. TEM images and their correlated particle size distribution of (a) Au and (b) Ag NPs.

Table 1. Average particle size and morphology of the synthesized particles.

Catalyst	*d* (nm)	Morphology
Au NPs	18.7 ± 8.8	spherical
Ag NPs	25.3 ± 10.1	anisotropic
Au40Ag NPs	25.4 ± 6.9	spherical core-shell

For the monometallic Ag NPs, the following is the reaction equation for the nucleation of Ag atoms(Saha et al., 2010):

$$12AgNO_3 + 4Na_3C_6H_5O_7 + 6H_2O \rightarrow 12Ag^0 + 12NaNO_3 + 4C_6H_8O_7 + 3O_2 \quad (4)$$

The synthesized Ag NPs have a bright yellow colour in solution (**Figure 1**) and were validated with the UV-Vis absorption measurement, which showed an SPR peak at 419 nm with a significant broadening (**Figure 2**). The spectra tail was also observed from the wavelength above 600 nm. The unique interaction of the free electrons of Ag NPs undergoes oscillations associated with the metal lattice in the presence of an oscillating electromagnetic field of light(Netala et al., 2018). These broadening of SPR with tail in the longer wavelength indicated that some particles were aggregated into bigger particles, and/or occupying with anisotropic morphology. TEM images further validated the findings that Ag NPs have sizes that vary greatly from 2 to 100 nm with various shapes, namely spherical, rods, and prisms (**Figure 3b**). These may be attributed to the fast-oxidation of AgNPs due to the O2 production that occurred in the reaction solution as stated in Equation (2). The oxygen may oxidise the Ag atoms produced back into Ag^+ ions, and the ions will eventually be deposited onto the surface of unoxidized Ag NPs. With the help of trisodium citrate as a ligand which is preferred to cover a certain facet of the Ag crystal, the anisotropic nanoparticles may eventually be produced. The reaction between ligands and Ag, for example, the binding of trisodium citrate on Ag shows preferential citric acid-binding, promoting crystal growth (Tang et al., 2014).

We also attempted to synthesize core-shell Au/Ag nanoparticles using the seeding method as suggested in the methodology section. The colour change was observed accordingly after the mixing process depending on the amount of Au seeds in the solution. The produced core-shell Au/Ag NPs depicted in **Figure 1**. The more Au seed in the solution, the more orange the colour produced.

UV-Vis absorption measurement of the core-shell Au/Ag NPs was depicted in **Figure 4**. Based on the spectrum, it can be seen that the amount of the Au seed as a core greatly influences the position and shape of the SPR. The thinner the Au core continuously causes the plasmon bands that appear to shift towards a lower wavelength, namely in the range of 389 to 460 nm which can be exclusively attributed to the

plasmon resonance of Ag particles. The decreasing concentration of Au core causes the resulting plasmon band to gradually decrease, which indicates the formation of composite particles with a larger diameter (Yang et al., 2008). Especially when we added 10 ml of core Au NPs, the SPR peaks started to have the second peak at the longer wavelength, and the most obvious peaks were observed when added 40 mL of Au seed formed core-shell Au40Ag NPs which have two peaks at 398 and 480 nm. The two spectral peaks produced by the two samples (Au20Ag and Au40Ag) indicate the difference in "shape" produced by the two core shells compared to the other samples. These separate peaks were 'finger print' for core-shell nanoparticles and significantly differed from alloy or monometallic nanoparticles. From the resulting absorbance spectrum, the difference in the resulting spectrum for all variations in skin thickness can be related that there was a reduction of Ag salts on the surface of the previously formed Au core and the shell structure of the composite nanoparticles is dominated by Ag shells. The complete list of the SPR peaks of the synthesized core-shell Au/Ag NPs is shown in **Table 2**. According to Feng et., al., 2019, two potential reasons affect the results obtained, namely: (1) If the Ag shell is thinner than the nucleus, it will be more active to encourage electron transfer in Au and Ag; (2) more electrons are transferred to compensate for the thinner Ag shell as compared to the thicker one.

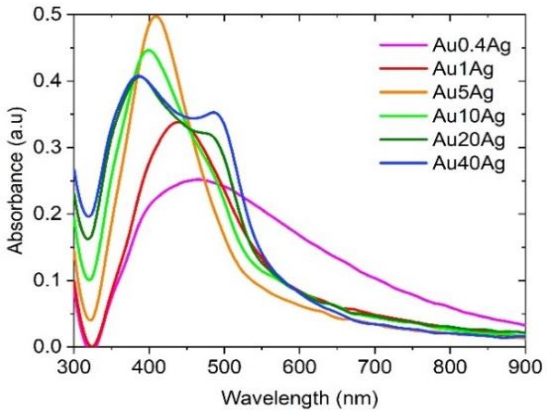

Figure 4. UV-vis absorbance spectra of Au/Ag core-shell (Au0.4Ag, Au1Ag, Au5Ag, Au10Ag, Au20Ag, and Au40Ag) NPs.

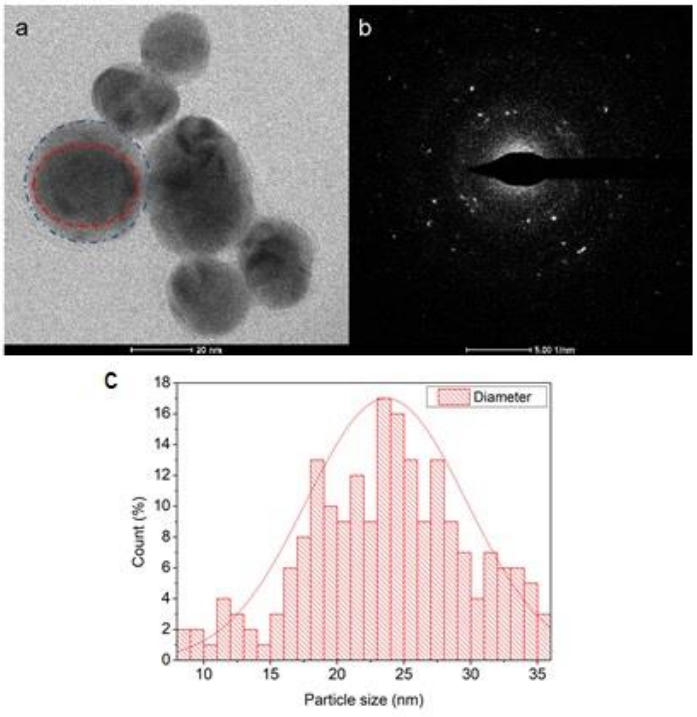

Figure 5. (a) TEM image, (b) the corresponding SAED pattern and (c) the particle size distribution of Au40Ag core-shell NPs

Table 2. SPR band position of Au, Ag and Au-Ag/core-shell NPs

No.	Sample	Volume (ml)		SPR (nm)
		Au seed	Ag^+	
1	Au NPs			520
2	Au 0.4Ag	0.4	1.2	465
3	Au1Ag	1	1.2	438
4	Au5Ag	5	1.2	409
5	Au10Ag	10	1.2	399
6	Au20Ag	20	1.2	385, 485
7	Au40Ag	40	1.2	385, 480
8	Ag NPs			419

Further, TEM observation revealed the core-shell structure of the Au/Ag NPs. Especially for Au40Ag NPs, TEM images showed two distinct areas in one particular nanoparticle, where Au as a core and Ag as a shell with various thicknesses of 2 - 5 nm (**Figure 5a**). The corresponding selected area electron diffraction (SAED) also validated the formation of the core-shell structure where the diffraction ring was seen to overlap between Au and Ag (**Figure 5b**).

The Reduction Reaction of 4-Nitrophenol with Nanoparticle Catalyst

In recent years, the reduction reaction of the harmful substance 4NP into the useful 4AP by sodium borohydride in an aqueous solution has become a model reaction that meets all criteria of a model reaction. Mixing with borohydride, 4NP produces a bright yellow solution of an intermediate product, namely 4-nitrophenolate ion, before being fully converted into 4AP (Bawarski et al., 2008; Kuroda et al., 2009). Because 4-nitrophenolate ions have strong absorption at 400 nm, the decay of this peak can be measured precisely using UV-Vis spectroscopy as a function of time (Verma et al., 2020). However, in the absence of a catalyst, the conversion rate of the 4NP to 4AP reaction by sodium borohydride is so small that the reaction should be monitored for hours. The metal catalyst has been explored for years to decrease the reaction time. Thus, the useful substances 4AP can be effectively obtained without delay, which is strategic from the industrial point of view.

We aimed to use this model reaction to test the catalytic performance of our synthesized nanoparticles. While there was an abundant study about the catalytic performance of noble monometallic NPs on this hydrogenation reaction, core-shell NPs have not been fully explored yet. Here, we will compare the catalytic performance between Au, Ag and core-shell Au/Ag NPs with similar sizes in the hydrogenation reaction of 4NP.

Figure 6 presented the UV-Vis absorption of 4NP before and after the addition of $NaBH_4$ for 100 μL. It can be seen from the figure, that the absorption peak of 4NP was shifted from 317 nm to 400 nm due to the formation of the 4-nitrophenolate ion. The colour of the mixture solution also changed from light yellow to bright one in the blink of an eye. In the absence of a catalyst, the reaction conversion is so slow that the colour is constant for up to 48 hours. When we added more borohydride ions into the mixture (**Figure 7**), the absorption peak at 400 nm decays rapidly. Still, no peak indicated to 4AP was observed, even when the added borohydride ions reach up to 4000 μL. Inset in **Figure 7** indicated that more borohydride ions added do not promote the conversion effectively.

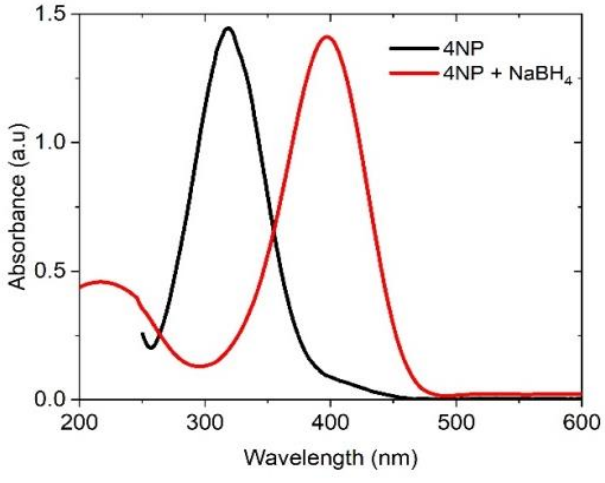

Figure 6. UV-vis absorption spectra of aqueous 4NP before (black) and after addition (red) of 100 μL $NaBH_4$

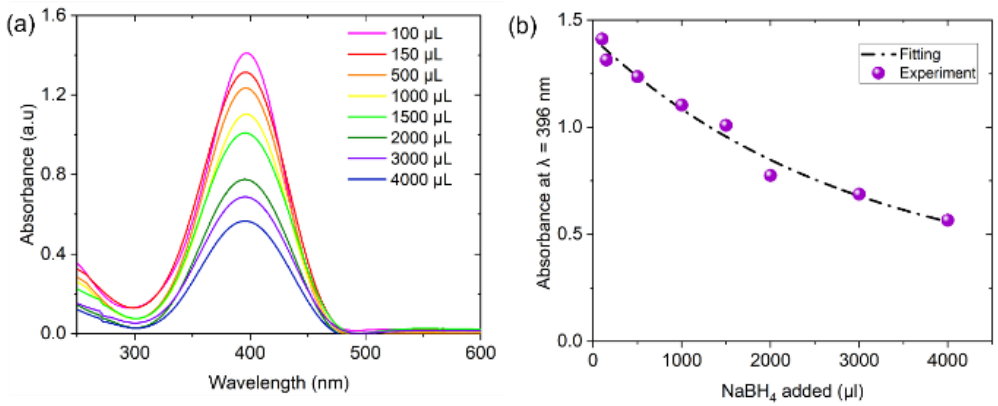

Figure 7. [**a**] UV-vis absorption spectra of 4NP reduced $NaBH_4$ in various concentrations. [**b**] Absorbance at 400 nm as a function of $NaBH_4$ concentration.

In the presence of NPS catalysts, the conversion phenomena are entirely different. **Figure 8** shows the UV-vis absorption spectra at different time points for the reduction of 4NP over citrate stabilized (**a**) Au, (**b**) Ag and (**c**) Au40Ag core-shell NPs. In general, all catalysts used in this work promoted the conversion significantly, as the absorption peak of 4AP was observed at 300 nm after some minutes the catalyst was added to the mixture assay. The reduction reaction was also visible through the colour change with bleaching of the yellow colour, indicating the complete conversion of 4NP. The decay of the 4-nitrophenolate absorption peak can also be seen more rapidly than those reactions without a catalyst. It is also worth noting that the isosbestic point was not observed in all reactions with catalyst. The missing isosbestic point can be attributed to H_2 gas involvement during the reaction, forming gas bubbles that disturb the absorbance measurement (Yamamoto et al., 2012). In the case of Au NPs, the reduction reaction was complete after 14 minutes at which the 4-nitrophenolate peak at 400 nm disappeared, while the new peak at 317 nm was observed and gradually increased time by time (**Figuer 8a**). For Ag NPs (**Figure 8b**), the reaction progressed slower than those for Au NPS as the peak at 400 nm seemed to be saturated at some point when the time was at 17 minutes, even though a small amount of 4AP can be obtained (low absorbance at 317 nm). In contrast to those monometallic counterparts, the reduction reaction of 4-NP was significantly progressed by the addition of core-shell Au40Ag NPs. **Figure 8c** illustrated that the reaction was completed within 11 minutes, indicated by the disappearance of the 4-nitrophenolate absorption peak at 400 nm and the significant appearance of 4-AP absorption peak at 317 nm.

The time dependence of the absorbance of 4-nitrophenolate ions at 400 nm for all reactions with catalyst can be characterized by plotting $ln(A_t/A_0)$ versus time shown in **Figure 9**. **Figure 9** shows the typical results of fitting Eq. (3) to the experimental $ln(A_t/A_0)(t)$ curves for all reaction 4-NP catalyst Au, Ag and Au40Ag NPs. It can be seen that the reduction reaction of 4-NP was fastly taken place when it was catalyzed with core-shell Au40Ag NPs indicated by a steep slope of the curve compared with those with Au or Ag NPs. In this case, the reaction rates were about 0.32757, 0.25686 and 0.05374 $minute^{-1}$ for Au40Ag, Au and Ag NPs, respectively (see **Table 2**). Interestingly, the reaction progressed similarly for Au and Au40Ag NPs, and 5 – 6 times faster if it is compared with the reaction catalyzed by Ag NPs. While the size of the synthesized nanoparticles and also crystallography properties between Au and Ag were quite similar, the variation in their catalytic properties was still in debate in the literature. The fact is that the Ag NPs always show poor catalytic activity against Au NPs, especially in the reduction of 4-NP (Verma, et al., 2020). In many literatures, it is stated that the reduction reaction of 4-NP into 4-AP by $NaBH_4$ in the presence of nanoparticles catalyst can be explained by the inherent hydrogen adsorption by the catalyst that transported the hydrogen to 4-NP, converting into 4-AP. In other words, metal NPs are known to catalyze this reaction by facilitating the electron transfer from BH_4^- to 4-NP. The efficiency of the catalyst is determined by the rate of the reaction, where a higher rate would indicate a better catalyst The observed difference in the catalytic activities among these synthesized nanostructures demonstrate the critical role of the Au core, which has superior catalytic performance. In our work, the reaction rate constant for reaction catalysized with Au40Ag core-shell NPs is slightly better than those with the similar structure synthesized by *Ananas comosus* leaves extract (Verma et al., 2020).

To describe the catalytic performance, there was also an induction period that generally (in most studies) correlated to the time for the metal catalyst surface to restructure due to the adsorption of hydrogen evolved in the solution(Menumerov et al., 2016; Zhao et al., 2015)(Menumerov et al., 2016; Zhao et al., 2015). The newest explanation of the induction period was ascribed by Strachan et al. as a phenomenon induced by the dissolved oxygen in the

system. They suggested that there is a buildup of the intermediates 4-nitrosophenol ($4NO^-$) during the catalysis, which can either be further reduced to 4-AP or, in the presence of the dissolved O_2, be oxidized to reform 4-NP. Simply by adding an inert argon gas to the system, the back oxidation of 4NO would not occur and thus, the related induction period would not be observed at all (Strachan et al., 2020). Strachan et al. also stated that the oxidation of the catalyst surface by the dissolved O_2 could give rise to the observed induction period. In our work, the reaction with a catalyst having the elemental Ag showed an induction period of about 2 minutes, while no induction period for those with Au NPs (**Table 2**). This result is in good agreement with the result by Strachan et al. and can be correlated to Ag NPs properties that are easily oxidized by the dissolved O_2. By allowing the catalyst and $NaBH_4$ to react with the dissolved O_2, the induction period is expected to decrease.

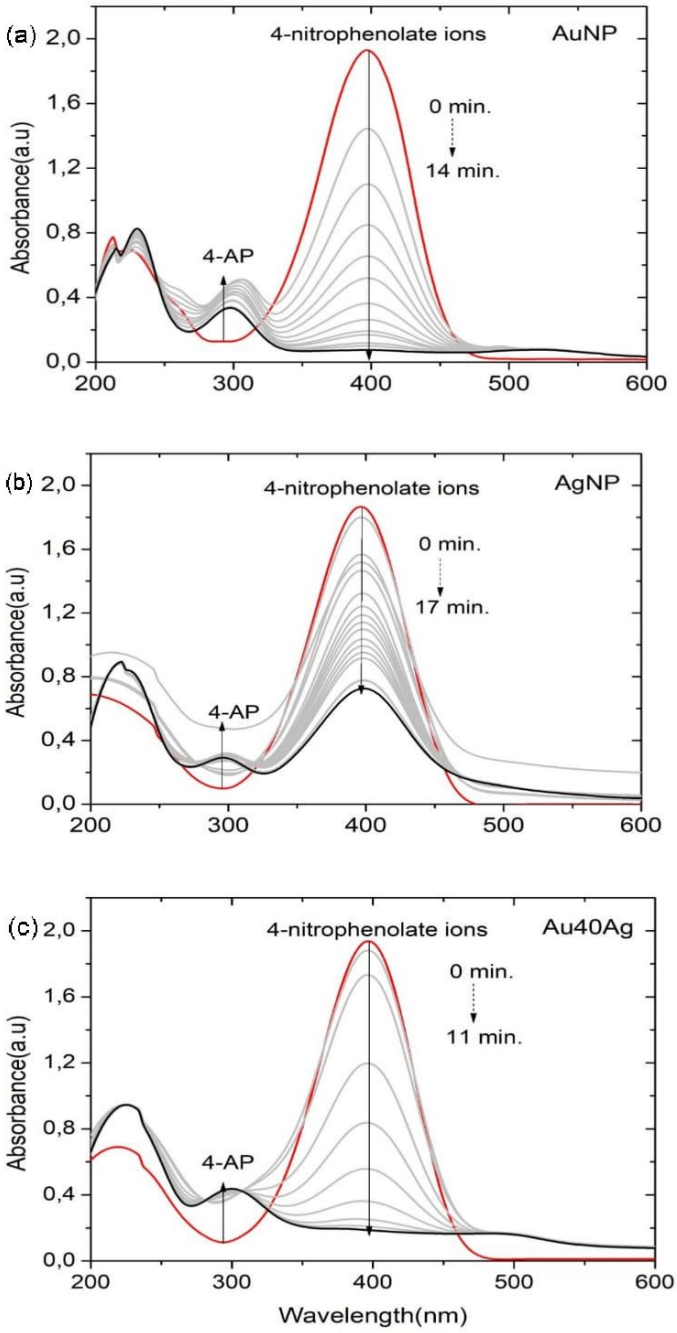

Figure 8. UV-vis absorption spectra at different time points for the reduction of 4NP over citrate stabilized (**a**) Au, (**b**) Ag and (**c**) Au40Ag core-shell NPs, with excess $NaBH_4$ in aqueous media at 298 K. Reaction condition; [4-NP] = 0.1 mM, [$NaBH_4$] = 17.24 mM, [catalyst] = 100 μL as prepared solution

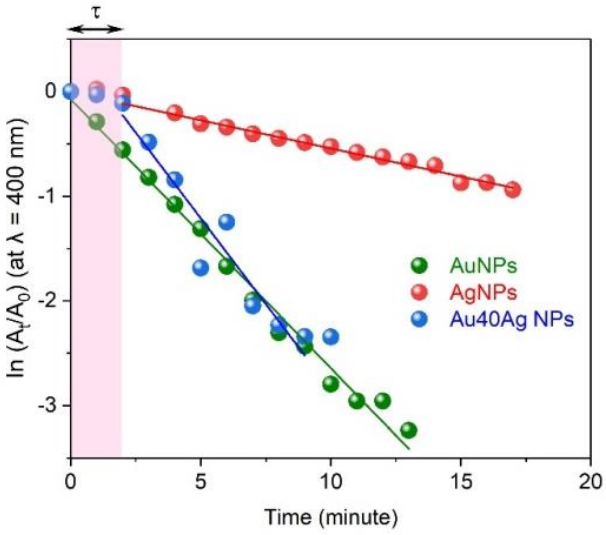

Figure 9. The plot of ln (A_t/A_0) versus time for reduction of 4NP to 4AP.

Table 3. Induction time and reaction rate constant

Catalyst	τ (minutes)	k_r (minute^{-1})	t (minutes)
Au NPs	0	0.25686	< 10
Ag NPs	2	0.05374	> 17
Au40Ag NPs	2	0.32757	< 8

To quantify the catalytic activity of nanoparticles, some works prefer to use turnover frequency, k_{TOF}, instead of the induction period or the reaction rate constant (Kästner & Thünemann, 2016). The turnover frequency is defined as the number of reactant molecules (4-NP) that 1 g of catalyst (metal NPS) can convert into a product (4-AP) per time. As we did not characterize the concentration of NPs in 100 μl we used in the reaction, we cannot define the TOF of our catalyst. Indeed, 100 μL of colloidal NPs used in a total reaction volume of 3 mL is quite excessive, as indicated by a small bump of SPR peak belonging to Au NPs at around 500 nm for both reaction catalyzed by Au and core-shell Au40Ag NPs, and a significant one in 400 nm belong to Ag NPs were observed in the time-dependent plot in **Figure 8a** and **8c** after the reaction completed. This claim was in good agreement with the colour of the solution after reaction which is still in the colour of the used catalyst, not a transparent one as for 4AP produced in the solution. Further work is needed to explore the effect of catalyst concentration on their catalytic performance and hence, reveal the TOF of the catalyst. Detailed characterization of solution after reaction using high-performance liquid chromatography (HPLC) and inductively coupled plasma (ICP) are expected to be important to quantify the 4AP product and the leftover catalyst so that the conversion and the catalyst efficiency can be defined.

CONCLUSIONS

In this study, an easy and simple synthesis process was carried out to produce Au, Ag, and Au-Ag/core-shell NPs. The resulting size and shape are quite uniform except for Ag nanoparticles with various shapes such as prisms and rods. The synthesized Au, Ag, and Au-Ag/core-shell NPs can be utilized as a good catalyst in reducing 4-NP to 4-AP in the presence of $NaBH_4$, with Au40Ag core-shell NPs having superior catalytic properties over the monometallic ones i.e. apparent rate constant is about 0.32757 min^{-1}. While the reaction with Au NPs catalyst had no induction period, the reaction with NPS catalyst containing elemental Ag had a large induction period (up to 2 minutes) due to dissolved O_2 consumption by both the intermediates produced and the catalyst itself (Ag is easy to be oxidized). Overall, this study shows that the chemical reduction method provides an easy and simple way of synthesizing Au and Ag NPs as well as the combination of the two, with excellent catalytic performance.

ACKNOWLEDGEMENTS

This study was supported by the national research grant of PN-MALSAI 2021 organized by Kedeputian IPK-LIPI. The authors would like to thank Ms. Siti Fadilah from TEM lab, Research Center for Physics BRIN, for collecting the beautiful TEM images of the nanoparticles.

AUTHOR CONTRIBUTIONSHIPS

Nurjannah: Data curation, Visualization, Formal analysis, Writing – original draft, Writing – review & editing. Bualkar Abdullah: Supervision, Validation. Yuliati Herbani: Conceptualization, Methodology, Formal Analysis, Visualization, Supervision, Resources, Validation, Reviewing and Editing.

REFERENCES

Aditya, T., Jana, J., Singh, N. K., Pal, A., & Pal, T. (2017). Remarkable facet selective reduction of 4-nitrophenol by morphologically tailored (111) faceted cu2o nanocatalyst. *ACS Omega*, *2*(5), 1968–1984. https://doi.org/10.1021/acsomega.6b00447

Ahmad, A. A. L., Panicker, S., Chehimi, M. M., Monge, M., Lopez-De-Luzuriaga, J. M., Mohamed, A. A., Bruce, A. E., & Bruce, M. R. M. (2019). Synthesis of water-soluble gold-aryl nanoparticles with distinct catalytic performance in the reduction of the environmental pollutant 4-nitrophenol. *Catalysis Science and Technology*, *9*(21), 6059–6071. https://doi.org/10.1039/c9cy01402k

Alshammari, T. M. (2016). Drug safety: The concept, inception and its importance in patients' health. *Saudi Pharmaceutical Journal*, *24*(4), 405–412. https://doi.org/10.1016/j.jsps.2014.04.008

Anugrah Ilahi, R., Firdaus, Ml., Amir, H., & Studi Pendidikan Kimia Jurusan PMIPA FKIP, P. (2021). Pemanfaatan nanopartikel emas (npe) sebagai pendeteksi kadar asam urat pada urine dengan metode citra digital (Utilization of gold nanoparticles (npe) as a detector of uric acid levels in urine with digital image method). *Jurnal Pendidikan Dan Ilmu Kimia*, *5*(2), 135–140.

Ayodhya, D., & Veerabhadram, G. (2019). Influence of g-C 3 N 4 and g-C 3 N 4 nanosheets supported CuS coupled system with effect of pH on the catalytic activity of 4-NP reduction using NaBH 4. *FlatChem*, *14*. https://doi.org/10.1016/j.flatc.2019.100088

Azhar, F. F. (2019). Pemanfaatan nanopartikel perak ekstrak belimbing wuluh sebagai indikator kolorimetri logam merkuri (Utilization of silver nanoparticles of star fruit extract as a colorimetric indicator of mercury metal). *Jurnal Ipteks Terapan*, *13*(1), 34. https://doi.org/10.22216/jit.2019.v13i1.3614

Bijalwan, K., Kainthola, A., Sharma, H., & Dwivedi, C. (2019). Catalytic reduction of 4-nitrophenol using gold-silver alloy nanoparticles coated on alkali-activated sand. *Materials Today: Proceedings*, *28*(2), 1097–1100. https://doi.org/10.1016/j.matpr.2020.01.089

Chiu, H. Y., Wi-Afedzi, T., Liu, Y. T., Ghanbari, F., & Lin, K. Y. A. (2020). Cobalt Oxides with Various 3D Nanostructured Morphologies for Catalytic Reduction of 4-Nitrophenol: A Comparative Study. *Journal of Water Process Engineering*, *37*(February), 101379. https://doi.org/10.1016/j.jwpe.2020.101379

Ciesielski, A., Skowronski, L., Górecka, E., Kierdaszuk, J., & Szoplik, T. (2018). Growth model and structure evolution of Ag layers deposited on Ge films. *Beilstein Journal of Nanotechnology*, *9*(1), 66–76. https://doi.org/10.3762/bjnano.9.9

Das, M., Shim, K. H., An, S. S. A., & Yi, D. K. (2011). Review on gold nanoparticles and their applications. In *Toxicology and Environmental Health Sciences*, 3(4), 193–205. Kluwer Academic Publishers. https://doi.org/10.1007/s13530-011-0109-y

Feng, Y., Wang, G., Chang, Y., Cheng, Y., Sun, B., Wang, L., Chen, C., & Zhang, H. (2019). Electron compensation effect suppressed silver ion release and contributed safety of Au@Ag Core-Shell Nanoparticles. *Nano Letters*, *19*(7), 4478–4489. https://doi.org/10.1021/acs.nanolett.9b01293

Haldar, K. K., Kundu, S., & Patra, A. (2014). Core-size-dependent catalytic properties of bimetallic Au/Ag core-shell nanoparticles. *ACS Applied Materials and Interfaces*, *6*(24), 21946–21953. https://doi.org/10.1021/am507391d

Hunge, Y. M., Yadav, A. A., Kang, S. W., Kim, H., Fujishima, A., & Terashima, C. (2021). Nanoflakes-like nickel cobaltite as active electrode material for 4-nitrophenol reduction and supercapacitor applications. *Journal of Hazardous Materials*, *419*(May), 126453. https://doi.org/10.1016/j.jhazmat.2021.126453

Ijaz, I., Gilani, E., Nazir, A., & Bukhari, A. (2020). Detail review on chemical, physical and green synthesis, classification, characterizations, and applications of nanoparticles. In *Green Chemistry Letters and Reviews 13* (3), pp. 59–81). Taylor and Francis Ltd. https://doi.org/10.1080/17518253.2020.1802517

Jana, J., Ganguly, M., & Pal, T. (2016). Enlightening surface plasmon resonance effect of metal nanoparticles for practical spectroscopic application. *RSC Advances*, *6*(89), 86174–86211. https://doi.org/10.1039/c6ra14173k

Jiang, X., Fan, X., Xu, W., Zhang, R., & Wu, G. (2020). Biosynthesis of Bimetallic Au-Ag Nanoparticles Using *Escherichia coli* and its Biomedical Applications. *ACS Biomaterials Science and Engineering*, *6*(1), 680–689. https://doi.org/10.1021/acsbiomaterials.9b01297

Kästner, C., & Thünemann, A. F. (2016). Catalytic Reduction of 4-Nitrophenol Using Silver Nanoparticles with Adjustable Activity. *Langmuir*, *32*(29), 7383–7391. https://doi.org/10.1021/acs.langmuir.6b01477

Khan, I., Saeed, K., & Khan, I. (2019). Nanoparticles: Properties, applications and toxicities. In *Arabian Journal of Chemistry* (Vol. 12, Issue 7, pp. 908–931). Elsevier B.V. https://doi.org/10.1016/j.arabjc.2017.05.011

Kosuda, K. M., Bingham, J. M., Wustholz, K. L., Van Duyne, R. P., & Groarke, R. J. (2019). Nanostructures and surface-enhanced Raman spectroscopy. In *Comprehensive Nanoscience and Nanotechnology* (Vols. 1–5, Issue August

2015). Elsevier Ltd. https://doi.org/10.1016/B978-0-12-803581-8.00611-1

Kuroda, K., Ishida, T., & Haruta, M. (2009). Reduction of 4-nitrophenol to 4-aminophenol over Au nanoparticles deposited on PMMA. *Journal of Molecular Catalysis A: Chemical*, *298*(1–2), 7–11. https://doi.org/10.1016/j.molcata. 2008.09.009

Kwizera, E. A., Chaffin, E., Shen, X., Chen, J., Zou, Q., Wu, Z., Gai, Z., Bhana, S., Oconnor, R., Wang, L., Adhikari, H., Mishra, S. R., Wang, Y., & Huang, X. (2016). Size- and shape-controlled synthesis and properties of magnetic-plasmonic core-shell nanoparticles. *Journal of Physical Chemistry C*, *120*(19), 10530–10546. https://doi.org/10.1021/acs.jpcc.6b00875

Mahalakshmi, G., Rajeswari, M., & Ponnarasi, P. (2020). Synthesis of few-layer g-C_3N_4 nanosheets-coated MoS_2/TiO_2 heterojunction photocatalysts for photo-degradation of methyl orange (MO) and 4-nitrophenol (4-NP) pollutants. *Inorganic Chemistry Communications*, *120*(July), 108146. https://doi.org/10.1016/j.inoche.2020.108146

Menumerov, E., Hughes, R. A., & Neretina, S. (2016). Catalytic reduction of 4-nitrophenol: a quantitative assessment of the role of dissolved oxygen in determining the induction time. *Nano Letters*, *16*(12), 7791–7797.https://doi.org/10.1021/acs.nanolett.6b03991

Mourya, M., Choudhary, D., Basak, A. K., Tripathi, C. S. P., & Guin, D. (2018). Ag-nanoparticles-embedded filter paper: an efficient dip catalyst for aromatic nitrophenol reduction, intramolecular cascade reaction, and Methyl Orange Degradation. *ChemistrySelect*, *3*(10), 2882–2887. https://doi.org/10.1002/slct.201702609

Neal, R. D., Inoue, Y., Hughes, R. A., & Neretina, S. (2019). Catalytic Reduction of 4-Nitrophenol by Gold Catalysts: The influence of borohydride concentration on the induction time [Research-article]. *Journal of Physical Chemistry C*, *123*(20), 12894–12901. https://doi.org/10.1021/acs.jpcc.9b02396

Nemanashi, M., & Meijboom, R. (2013). Synthesis and characterization of Cu, Ag and Au dendrimer-encapsulated nanoparticles and their application in the reduction of 4-nitrophenol to 4-aminophenol. *Journal of Colloid and Interface Science*, *389*(1), 260–267. https://doi.org/10.1016/j.jcis.2012.09.012

Netala, V. R., Bukke, S., Domdi, L., Soneya, S., G. Reddy, S., Bethu, M. S., Kotakdi, V. S., Saritha, K. V, & Tartte, V. (2018). Biogenesis of silver nanoparticles using leaf extract of Indigofera hirsuta L. and their potential biomedical applications (3-in-1 system). *Artificial Cells, Nanomedicine, and Biotechnology*, *46*(sup1), 1138–1148. https://doi.org/10.1080/21691401.2018.1446967

Primo, A., & García, H. (2013). Supported gold nanoparticles as heterogeneous catalysts. *New and Future Developments in Catalysis: Catalysis by Nanoparticles*, 425–449. https://doi.org/10.1016/B978-0-444-53874-1.00019-6

Rahman, M. M. (2020). Selective and sensitive 4-Aminophenol chemical sensor development based on low-dimensional Ge-doped ZnO nanocomposites by electrochemical method. *Microchemical Journal*, *157*. https://doi.org/10.1016/j.microc.2020.104945

Ren, H., Yang, J. L., Yang, W. M., Zhong, H. L., Lin, J. S., Radjenovic, P. M., Sun, L., Zhang, H., Xu, J., Tian, Z. Q., & Li, J. F. (2021). Core-shell-satellite plasmonic photocatalyst for broad-spectrum photocatalytic water splitting. *ACS Materials Letters*, *3*(1), 69–76. https://doi.org/10.1021/acsmaterialslett.0c00479

Sabourian, P., Yazdani, G., Ashraf, S. S., Frounchi, M., Mashayekhan, S., Kiani, S., & Kakkar, A. (2020). Effect of physico-chemical properties of nanoparticles on their intracellular uptake. *International Journal of Molecular Sciences*, *21*(21), 1–20. https://doi.org/10.3390/ijms21218019

Sahu, K., Singhal, R., & Mohapatra, S. (2020). Morphology controlled cuo nanostructures for efficient catalytic reduction of 4-nitrophenol. *Catalysis Letters*, *150*(2), 471–481. https://doi.org/10.1007/s10562-019-03009-w

Salvioni, L., Morelli, L., Ochoa, E., Labra, M., Fiandra, L., Palugan, L., Prosperi, D., & Colombo, M. (2021). The emerging role of nanotechnology in skincare. *Advances in Colloid and Interface Science*, *293*, 102437. https://doi.org/10.1016/j.cis.2021.102437

Sarmah, P., Deka, P., & Bharali, P. (2015). *Catalytic reduction of 4-nitrophenol to 4-aminophenol over CuNi alloy particles : Synthesis , characterization and application*. *12*(January 2013), 54–60.

Shen, W., Qu, Y., Pei, X., Li, S., Yu, S., Wang, J., Zhang, Z., & Zhou, J. (2017). Catalytic reduction of 4-nitrophenol using gold nanoparticles biosynthesized by cell-free extracts of Aspergillus sp. WL-Au. *Journal of Hazardous Materials*, *321*, 299–306. https://doi.org/10.1016/j.jhazmat.2016.07.051

Strachan, J., Barnett, C., Masters, A. F., & Maschmeyer, T. (2020). 4-Nitrophenol Reduction: Probing the putative mechanism of the model reaction. *ACS Catalysis*, *10*(10), 5516–5521. https://doi.org/10.1021/acscatal.0c00725

Stratakis, E., & Kymakis, E. (2013). Nanoparticle-based plasmonic organic photovoltaic devices. *Materials Today*, *16*(4), 133–146.

https://doi.org/10.1016/j.mattod.2013.04.006

Tang, Z., Zhang, Q., Yin, Y., & Chang, C. E. A. (2014). Facet selectivity of ligands on silver nanoplates: Molecular mechanics study. *Journal of Physical Chemistry C*, *118*(37), 21589–21598. https://doi.org/10.1021/jp503319s

Umamaheswari, C., Lakshmanan, A., & Nagarajan, N. S. (2018). Green synthesis, characterization and catalytic degradation studies of gold nanoparticles against congo red and methyl orange. *Journal of Photochemistry and Photobiology B: Biology*, *178*, 33–39. https://doi.org/10.1016/j.jphotobiol.2017.10.017

Verma, V., Singh, M., Pal Singh, P., Singh, J., & Rawat, M. (n.d.). *Highly stable Au/Ag core-shell nanoparticles prepared via novel green approach for the abatement of nitro pollutants*. https://doi.org/10.1049/mnl.2020.0275

Vinod, M., & Gopchandran, K. G. (2014). Au, Ag and Au: Ag colloidal nanoparticles synthesized by pulsed laser ablation as SERS substrates. *Progress in Natural Science: Materials International*, *24*(6), 569–578. https://doi.org/10.1016/j.pnsc.2014.10.003

Vishwakarma, V., & Uthaman, S. (2019). Environmental impact of sustainable green concrete. In *Smart Nanoconcretes and Cement-Based Materials: Properties, Modelling and Applications* (pp. 241–255). Elsevier Inc. https://doi.org/10.1016/B978-0-12-817854-6.00009-X

Wang, K., Sun, D. W., Pu, H., & Wei, Q. (2019). Shell thickness-dependent Au@Ag nanoparticles aggregates for high-performance SERS applications. *Talanta*, *195*, 506–515. https://doi.org/10.1016/j.talanta.2018.11.057

Wi-Afedzi, T., Yeoh, F. Y., Yang, M. T., Yip, A. C. K., & Lin, K. Y. A. (2019). A comparative study of hexacyanoferrate-based Prussian blue analogue nanocrystals for catalytic reduction of 4-nitrophenol to 4-aminophenol. *Separation and Purification Technology*, *218*(February), 138–145. https://doi.org/10.1016/j.seppur.2019.02.047

Wumaer, M., Abdulla, R., Kou, Y., Liu, Z., Akram, N., Aisa, H. A., & Wang, J. (2022). Establishment of integrated analysis method for probing and reconstructing hydrogenation mechanism of a model reaction. *Catalysts*, *12*(5), 499; https://doi.org/10.3390/catal12050499

Yahya, A. A., Rashid, K. T., Ghadhban, M. Y., Mousa, N. E., Majdi, H. S., Salih, I. K., & Alsalhy, Q. F. (2021). Removal of 4-nitrophenol from aqueous solution by using polyphenylsulfone-based blend membranes: Characterization and performance. *Membranes*, *11*(3), 1–20. https://doi.org/10.3390/membranes11030171

Yamamoto, H., Yano, H., Kouchi, H., Obora, Y., Arakawa, R., & Kawasaki, H. (2012). N,N-Dimethylformamide-stabilized gold nanoclusters as a catalyst for the reduction of 4-nitrophenol. *Nanoscale*, *4*(14), 4148–4154. https://doi.org/10.1039/c2nr30222e

Yang, Y., Shi, J., Kawamura, G., & Nogami, M. (2008). Preparation of Au-Ag, Ag-Au core-shell bimetallic nanoparticles for surface-enhanced Raman scattering. *Scripta Materialia*, *58*(10), 862–865. https://doi.org/10.1016/j.scriptamat.2008.01.017

Yu, Z., Moussa, H., Liu, M., Schneider, R., & Wang, W. (2021). Development of photocatalytically active heterostructured MnO/ZnO and CuO/ZnO films via solution precursor plasma spray process Surface and Coatings Technology *371*, 107-116. https://doi.org/10.1016/j.surfcoat.2019.02.053

Zhao, P., Feng, X., Huang, D., Yang, G., & Astruc, D. (2015). Basic concepts and recent advances in nitrophenol reduction by gold- and other transition metal nanoparticles. *Coordination Chemistry Reviews*, *287*, 114–136. https://doi.org/10.1016/j.ccr.2015.01.002